Phase-slope and group-dispersion calculations in the frequency domain by simple optical low-coherence reflectometry

Young L. Kim, Joseph T. Walsh, Jr., and Matthew R. Glucksberg

We report a new method by which phase slope and group dispersion can be calculated with a simple optical low-coherence reflectometer to quantify physiological conditions. A discrete-time signal processing algorithm based on the first and second derivatives of the phase with respect to wave number was developed from discrete-time Fourier properties. The algorithm avoids the 2π ambiguity associated with most phase unwrapping. Experimental data collected by use of well-characterized optical materials validated the algorithm, which was minimally sensitive to phase noise. The group dispersion of bovine cornea was measured at various hydrations and was significantly dependent on hydration. The results suggest that group dispersion is an indicator of corneal alterations. © 2003 Optical Society of America

OCIS codes: 070.6020, 260.2030, 120.5050, 120.3180, 170.4500.

1. Introduction

Optical coherence tomography (OCT) and optical low-coherence reflectometry (OLCR) have been used to image spatial variations in sample intensity,[1–3] velocity,[4,5] polarization properties,[6–8] spectral properties,[9] and mechanical properties.[10] Our study is focused on the measurement of optical properties such as dispersion for the quantification of the physiological states of biological tissues (e.g., hydration). Previously, refractive indices were determined by measurement of the physical and optical path lengths of a sample.[11,12] Group dispersion was estimated by measurement of changes in group refractive index with two light sources, assuming that group dispersion was linear in the spectral region 810–860 nm.[13]

Several properties of OCT or OLCR interference signals depend on the spectrum of the light source. The axial resolution is inversely proportional to the spectral width of the light. For example, for a Ti:Al_2O_3 laser with a 145-nm spectral bandwidth, resolution as high as 1.9 μm was demonstrated.[14] In dispersive media such as biological tissues, however, different wavelengths of a broadband light source have different velocities.[15] Dispersion is known to increase the width of the envelope and to reduce the resolution in an OCT image. By use of a dispersion-compensating element in the reference arm[16] or of a deconvolution method,[17] resolution in OCT images has been enhanced. However, when the dispersion properties of samples vary locally, these methods cannot be applied to improve resolution. A digital algorithm that uses a dispersion model was developed to correct dispersion and produced an enhanced OCT image.[18] A stable and reproducible inference signal was obtained by means of an electro-optical phase modulator, and broadening of the inference signal was corrected by group-dispersion compensation in a rapid-scanning optical delay line.[19]

We demonstrate the quantification of phase slope and group dispersion from an interference signal in the frequency domain by use of discrete-time signal processing with a single-light-source OLCR system. The first and the second derivatives of the phase of the interference signal with respect to wave number can be calculated from Fourier-transform properties. First, we show that the shift of the phase slope of the interior to that of the posterior surface of a sample represents the optical thickness of the sample. Second, the group dispersion of the sample is extracted from the second derivative of the phase. Experimental data collected for water and zinc selinde

The authors are with the Department of Biomedical Engineering, Northwestern University, Evanston, Illinois 60208. Y. L. Kim's e-mail address is younglae@northwestern.edu.

Received 14 March 2003; revised manuscript received 8 September 2003.

0003-6935/03/346959-08$15.00/0

(ZnSe) are used to validate the algorithm. Finally, as a biological example, the group dispersion of bovine cornea is calculated under various hydration conditions.

2. Theory

The phase of the interference signal can be expanded about the wavelength in a Taylor series.[20] The phase, $\phi(k)$, is given by $\phi(k) = kn_p(k)z$, where k is the wave number ($k = 2\pi/\lambda$; λ is the wavelength), n_p is the wavelength-dependent phase refractive index, and z is the geometrical path-length difference between the two arms of the interferometer. Expanding, $\phi(k) = \phi(k_s) + (k - k_s)[d\phi(k_s)/dk] + [(k - k_s)^2/2](d^2\phi(k_s)/dk^2) + \ldots$, where k_s is the central wave number of a light source. If the light source is monochromatic, that is, if $k = k_s$, only the first term remains, such that $\phi(k) = \phi(k_s) = k_s n_p(k_s)z$. In quasi-monochromatic or broadband light sources, the first derivative of the phase about the wave number, $d\phi(k_s)/dk$, becomes $d\phi(k_s)/dk = n_g(k_s)z$ because $n_g = n_p + k(dn_p/dk)$, where n_g is the group refractive index. The product of n_g and z is the optical distance in the quasi-monochromatic light source. However, in standard OCT or OCLR, accurate detection of the phase is difficult because of the presence of noise caused by the scanning system, the data acquisition board, and mechanical vibration of the optical table.[21,22]

A. Phase Slope Calculation Algorithm

To find the phase slope, $d\phi/dk$, one must find the phase as a function of wave number and take the derivative of the phase with respect to the wave number. Mathematically, the phase may be found from the Fourier transformation of the interference signal. The phase is given by

$$\phi(k) = \tan^{-1}\left(\frac{\mathrm{Im}[\mathrm{FT}\{I[n]\}]}{\mathrm{Re}[\mathrm{FT}\{I[n]\}]}\right), \tag{1}$$

where FT{ } denotes the Fourier transformation, $I[n]$ is the intensity at the detector, and n is the sequence of the discrete-time signal. However, this method requires a phase-unwrapping algorithm because of the 2π ambiguity. The difficulty of dealing with the 2π ambiguity can be avoided in the following discrete-time signal processing algorithm. First, if we let $\mathcal{J}(e^{iw})$ be the Fourier transform of $I[n]$, then $\mathcal{J}(e^{iw})$ is expressed by

$$\mathcal{J}(e^{iw}) = |\mathcal{J}(e^{iw})|\exp\{i\ \arg[\mathcal{J}(e^{iw})]\}, \tag{2}$$

where $|\mathcal{J}(e^{jw})|$ is the magnitude of the Fourier transform, $\arg[\mathcal{J}(e^{jw})]$ is its phase, and w is the angular frequency of the interference signal. Second, $\hat{\mathcal{J}}(e^{iw})$ is defined such that

$$\hat{\mathcal{J}}(e^{iw}) \equiv \log\ \mathcal{J}(e^{iw}) = \log|\mathcal{J}(e^{iw})| + i\ \arg[\mathcal{J}(e^{iw})]. \tag{3}$$

{If we define $\hat{I}[n]$ as the inverse Fourier transform of $\hat{\mathcal{J}}(e^{iw})$, the sequence $\hat{I}[n]$ is commonly referred to as the complex cepstrum of $I[n]$.} Then the derivative of $\hat{\mathcal{J}}(e^{iw})$ is

$$\frac{d\hat{\mathcal{J}}(e^{iw})}{dw} = \frac{d[\log\ \mathcal{J}(e^{iw})]}{dw} = \frac{d\mathcal{J}(e^{iw})/dw}{\mathcal{J}(e^{iw})}, \tag{4}$$

where $d\mathcal{J}(e^{iw})/dw$ in the numerator can be calculated by a Fourier-transform theorem[24]:

$$\begin{aligned}\frac{d\mathcal{J}(e^{iw})}{dw} &= \frac{d}{dw}\left[\sum_{n=-\infty}^{\infty} I[n]\exp(-iwn)\right] \\ &= -i\sum_{n=-\infty}^{\infty} nI[n]\exp(-iwn) \\ &= -i\mathrm{FT}\{nI[n]\}.\end{aligned} \tag{5}$$

When Eq. (5) is substituted into Eq. (4), phase derivative $d\phi/dw$, which is the imaginary part of $d\hat{\mathcal{J}}(e^{iw})/dw$, becomes

$$\frac{d\phi}{dw} = \mathrm{Im}\left[\frac{d\hat{\mathcal{J}}(e^{iw})}{dw}\right] = \mathrm{Im}\left[\frac{-i\mathrm{FT}\{nI[n]\}}{\mathcal{J}(e^{iw})}\right]. \tag{6}$$

Phase slope $d\phi/dk$ is then calculated from $d\phi/dw$, which is calculated by use of the chain rule:

$$\frac{d\phi}{dk} = \frac{d\phi}{dw}\frac{dw}{dk} = 2V\frac{d\phi}{dw}, \tag{7}$$

where $dw/dk = 2V$ because $w = d\phi/dt = d(kn_g z)/dt = k(2V)$, V is the scanning speed of the mirror in the reference arm, and the factor 2 comes from a round trip in the Michelson interferometer. Let us consider the conversion of a continuous-time signal, $x_c(t)$, to a discrete-time signal, $x_s(t)$, through modulation of $s(t) = \sum_{n=-\infty}^{\infty}\delta(t - n)$, where δ is a Dirac delta function and n is an integer. Then $x_s(t) = s(t/T_s)x_c(t)$, where $T_s = 1/f_s$ is the sampling period. The Fourier transformation of $x_s(t)$ is $\mathrm{FT}\{x_s(t)\} = \mathrm{FT}\{s(t/T_s)\} * \mathrm{FT}\{x_c(t)\} = T_s s(T_s t) * \mathrm{FT}\{x_c(t)\}$, where $*$ is the convolution operation because $\mathrm{FT}\{s(t/T_s)\} = T_s s(T_s t)$.[25] Thus the slope, $d\phi/dk$, must be rescaled by $1/f_s$ to be expressed as a discrete-time signal. Finally, phase slope $d\phi/dk$ in discrete time becomes

$$\frac{d\phi}{dk} = \frac{2V}{f_s}\frac{d\phi}{dw} = \frac{2V}{f_s}\mathrm{Im}\left[\frac{-i\mathrm{FT}\{nI[n]\}}{\mathcal{J}(e^{iw})}\right], \tag{8}$$

where $2V/f_s$ is also the distance interval of each sampled point.

B. Group-Dispersion Calculation Algorithm

The following algorithm for calculating group dispersion, based on the first and the second derivatives of the phase, are derived by use of basic discrete-time Fourier-transform properties. The group dispersion, $dn_g/d\lambda$, can be calculated from the chain rule:

$$\frac{dn_g}{d\lambda} = -\frac{1}{z}\frac{2\pi}{\lambda^2}\frac{d^2\phi}{dk^2}, \tag{9}$$

based on $n_p = (\lambda/2\pi)(\phi/z)$. Then $d^2\phi/dk^2$ is calculated as follows: First, from Eq. (4), the second derivative of $\hat{\mathcal{F}}(e^{iw})$ is

$$\frac{d^2\hat{\mathcal{F}}(e^{iw})}{dw^2} = \frac{d}{dw}\left\{\frac{d[\log \mathcal{F}(e^{iw})]}{dw}\right\} = \frac{d}{dw}\left[\frac{d\mathcal{F}(e^{iw})/dw}{\mathcal{F}(e^{iw})}\right] = \frac{d^2\mathcal{F}(e^{iw})/dw^2}{\mathcal{F}(e^{iw})} - \left[\frac{d\mathcal{F}(e^{iw})/dw}{\mathcal{F}(e^{iw})}\right]^2, \quad (10)$$

where $d^2\mathcal{F}(e^{iw})/dw^2$ is calculated by the definition of the discrete-time Fourier transform such that

$$\frac{d^2\mathcal{F}(e^{iw})}{dw^2} = \frac{d^2}{dw^2}\left[\sum_{n=-\infty}^{\infty} I[n]\exp(-iwn)\right] = -\sum_{n=\infty}^{\infty} n^2 I[n]\exp(-iwn) = -\mathrm{FT}\{n^2 I[n]\}. \quad (11)$$

Substituting Eqs. (5) and (11) into Eq. (10) yields as the second derivative of $\hat{\mathcal{F}}(e^{iw})$

$$\frac{d^2\hat{\mathcal{F}}(e^{iw})}{dw^2} = \frac{-\mathrm{FT}\{n^2 I[n]\}}{\mathcal{F}(e^{iw})} - \left[\frac{-i\mathrm{FT}\{nI[n]\}}{\mathcal{F}(e^{iw})}\right]^2. \quad (12)$$

The second derivative of the phase, $d^2\phi/dw^2$, is the imaginary part of $d^2\hat{\mathcal{F}}(e^{iw})/dw^2$:

$$\frac{d^2\phi}{dw^2} = \mathrm{Im}\left[\frac{d^2\hat{\mathcal{F}}(e^{iw})}{dw^2}\right] = \mathrm{Im}\left\{\frac{-\mathrm{FT}\{n^2 I[n]\}}{\mathcal{F}(e^{iw})} - \left[\frac{-i\ \mathrm{FT}\{nI[n]\}}{\mathcal{F}(e^{iw})}\right]^2\right\}. \quad (13)$$

Then, the second derivative of the phase with respect to the wave number, $d^2\phi/dk^2$, in the discrete time becomes

$$\frac{d^2\phi}{dk^2} = \left(\frac{2V}{f_s}\right)^2 \frac{d^2\phi}{dw^2} = \left(\frac{2V}{f_s}\right)^2 \mathrm{Im}\left(\frac{-\mathrm{FT}\{n^2 I[n]\}}{\mathcal{F}(e^{iw})} - \left[\frac{-i\mathrm{FT}\{nI[n]\}}{\mathcal{F}(e^{iw})}\right]^2\right). \quad (14)$$

Finally, substituting Eq. (14) into Eq. (9) yields group dispersion $dn_g/d\lambda$:

$$\frac{dn_g}{d\lambda} = -\frac{2\pi}{z\lambda^2}\left(\frac{2V}{f_s}\right)^2 \mathrm{Im}\left(\frac{-\mathrm{FT}\{n^2 I[n]\}}{\mathcal{F}(e^{iw})} - \left[\frac{-i\mathrm{FT}\{nI[n]\}}{\mathcal{F}(e^{iw})}\right]^2\right). \quad (15)$$

3. Materials and Methods

A. System Description

The light source was a superluminescent diode (SLD; Superlum, Ltd., Moscow) with a central wavelength, λ_s, of 819.9 nm, a specified full width spectral bandwidth $\Delta\lambda$ of 21.9 nm at half-maximum, a spectral ripple of 0.4%, and a maximum output power of 1.80 mW at 140-mA SLD current. The coherence length of the interference signal, which is defined by a full width of the interference signal at half-maximum, was measured with a mirror in the sample arm. The measured coherence length was 18 μm, close to theoretical coherence length: $l_c = (2\ln 2/\pi)(\lambda_s{}^2/\Delta\lambda) = 16.5$ μm. The current and the temperature of the SLD were controlled by a PILOT-2 Driving Set (Superlum, Ltd.). The light passed through an optical fiber into a 50/50 coupler (Fiber Optic Network Technology Company, Surrey, British Columbia, Canada), which split the light into a reference arm and a sample arm (see Fig. 1). The light in each arm was collimated by an aspheric lens (350230-B; Thorlabs, Inc., Newton, New Jersey) placed immediately after the end of the optical fiber. The light in the reference arm was reflected by a corner-cube retroreflector (Edmund Scientific Company, Barrington, New Jersey) mounted upon a voice coil scanning system (Model V-102.1L QuickScan; Physik Instrumente, Waldbronn, Germany). The scanning speed of the voice coil scanning system was set at 16 mm/s, corresponding to a 39-kHz modulation frequency. In the sample arm the light was reflected by the internal structures of a sample. The light reflected from the sample arm and the light from the reference arm were recombined at a photodetector (Model 2011; New Focus, Inc., Santa Clara, California). The detector passband was set to pass signals from 30 to 100 kHz. A data acquisition board (Model AT-MIO-16E-1; National Instruments, Austin, Texas) sampled the signals with $f_s = 1$ MHz into a computer.

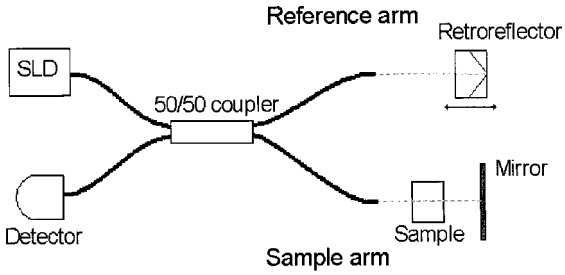

Fig. 1. Experimental setup for the group-dispersion algorithm. Half of the light from the SLD goes to the reference arm; half goes to the sample arm. Reflected light from both arms interferes and is sensed at the detector. The interference signal formed by the light reflected from the coated mirror and the retroreflector is processed for calculating the group dispersion.

B. Phase Slope

We tested the phase slope calculation algorithm with a 1.02-mm-thick microscope slide (Fisher Scientific, Pittsburgh, Pennsylvania, $n_g = 1.516$ at 820 nm) to verify that the optical thickness equals the shift of the phase slope of the anterior interference signal (air–glass interface) and that of posterior interference signal (glass–air interface) in the frequency domain. In the time domain the optical thickness, which is the

product of the geometrical thickness and the group refractive index, was observed as the distance between two peaks of the envelope signal demodulated with quadrature-amplitude demodulation. In the frequency domain, the shift of the phase slope calculated by the algorithm was compared with the optical thickness.

C. Group Dispersion

We used water in a 1-cm-thick cuvette to measure the group dispersion of water, as shown in Fig. 1. First, an empty cuvette (1-cm inside thickness) was placed immediately before a metallic mirror (coating for IR from the Newport Company, Irvine, California). Because the antireflection coating on the mirror can be dispersive in itself, one should take the dispersion of the antireflection coating on the mirror into account to calculate accurate dispersion of the sample. We assume that the total dispersion effect of the sample and the antireflection coating of the mirror is a linear superposition of each dispersion effect. One hundred *A* scans of the reflection from the coated mirror through the empty cuvette were collected for group dispersion of the mirror. The cuvette then was filled with distilled water, and 100 *A* scans of the reflection from the coated mirror through the water-filled cuvette were collected for the total group dispersion. By subtracting the group dispersion of the mirror from the total group dispersion, we eliminated the dispersion effect of the antireflection coating on the mirror. Three main peaks appeared in the time domain: one at the anterior cuvette–water interface, one at the posterior water–cuvette interface, and one at the air–mirror interface. We processed the interference signal from the mirror instead of the signal from the posterior interface to calculate the group dispersion of the sample by using the group-dispersion-calculation algorithm because the mirror generated a strong reflection. As a second test of the group-dispersion calculation, a 2.08-mm-thick ZnSe disk (Wilmad Glass Company, Inc., Buena, New Jersey; $n_g = 2.60$ at 820 nm) was utilized. One hundred *A* scans were collected with and then without the ZnSe disk, which was placed immediately before the coated mirror in the sample arm. The group-dispersion algorithm was applied to produce the group dispersion of ZnSe.

To study the relationship between the group dispersion and hydration as the quantification of the physiological state of a biological tissue we measured the group dispersion of bovine cornea under various hydration conditions. Four calf eyes were collected from a local slaughterhouse. The eyes were brought to our laboratory within 1 h post-mortem. The corneal epithelium was removed by scraping with a surgical blade (Feather Safety RaZor Company, Ltd., Osaka, Japan). To increase the corneal hydration initially, we placed each eye in a beaker containing 50 mL of physiological saline solution (0.9% NaCl solution) for various periods (from 2 to 4 h), which determined initial hydration. A 10-mm-diameter disk was cut from the center of the cornea. To obtain uniform hydration across the thickness we placed each corneal disk into a closed chamber for 12 to 24 h, thereby dehydrating the corneas at a slow rate. The chamber contained a saturated aqueous solution of K_2SO_4; thus a constant relative humidity of 97% was generated at 25 °C.[26] Next, the cornea was placed in a holder that was designed to maintain the shape of the cornea before the coated mirror. Two or three sets of 100 *A* scans were collected. Immediately after data collection, the cornea was removed from the holder and 100 *A* scans of the coated mirror without the corneal disk were collected as a reference. In addition, the geometrical thickness and the group refractive index were calculated by the method proposed by Sorin and Gray.[11] The geometrical thickness and the group refractive index can be determined simultaneously by measurement of the optical thickness and the difference between the optical thickness and the geometrical thickness of the sample. Because the cornea's thickness is linearly proportional to its hydration, the corneal hydration was estimated from the corneal thickness.[27] Corneal hydration H was converted from corneal thickness T (in micrometers) from the formula $H = 5.3 \times 10^{-3} \times T - 0.67$.[28] The corneal hydration was determined experimentally from the ratio of the measured weight of water content to the measured weight of the completely dehydrated cornea.

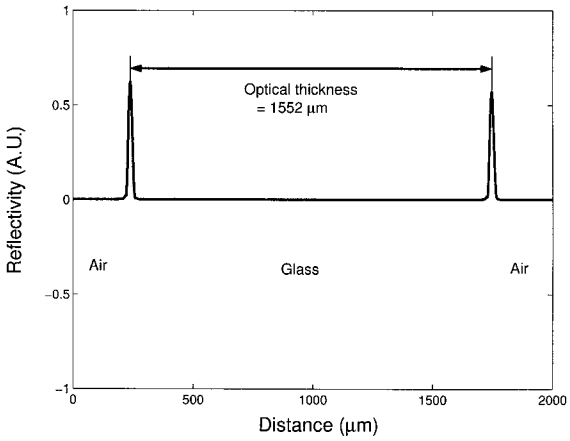

Fig. 2. *A* scan of the microscope slide in the time domain. The lighter curve represents the interference signal, and the darker curve is the envelope of the signal obtained by quadrature-amplitude demodulation.

4. Results

A. Phase Slope

To demonstrate the accuracy of the phase-slope calculation we quantified the optical thickness of a microscope slide, using both time- and frequency-domain methods. Figure 2 shows two peaks, one from the air–glass interface and the other from the glass–air interface, in the time domain. The optical thickness measured in the time domain was 1552 μm, as shown in Fig. 2. This thickness is the product of the group refractive index and the geometrical

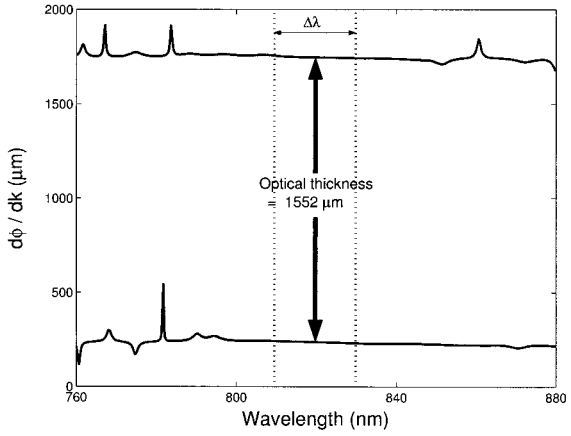

Fig. 3. Phase slope $d\phi/dk$ in the frequency domain. The shift in the phase slope at the central wavelength, $\lambda = 820$ nm, is the optical thickness of the microscope slide.

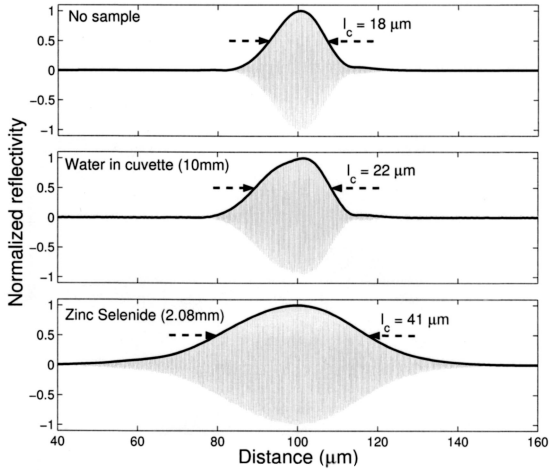

Fig. 4. Interference signals from the coated mirror through three samples in the sample arm. Top, *A* scan without a sample. Coherence length l_c is 18 μm, close to the theoretical coherence length of 16.5 μm. Center, *A* scan with the cuvette filled with water (10-mm inside thickness). Coherence length l_c, is 22 μm. Bottom, *A* scan of a 2.08-mm-thick ZnSe disk. Coherence length l_c is 41 μm.

thickness. To quantify optical thickness based on frequency-domain calculations we calculated phase slopes $d\phi/dk$ of the first interference signal (air–glass interface) and the second interference signal (glass–air interface), using Eq. (8). Each interference peak was analyzed according to Eq. (8) with a 2^{11}-point-long, 66-μm-long rectangular window centered on each peak. The optical thickness was the shift of the phase slopes (see Fig. 3) such that

$$\left.\frac{d\phi}{dk}\right|_{\text{glass–air}} - \left.\frac{d\phi}{dk}\right|_{\text{air–glass}} = Tn_g = 1552\ \mu\text{m},$$

where T is the geometrical thickness and n_g is the group refractive index of the microscope slide. The x axis of Fig. 3 was generated such that $\lambda = 2V/f$, where $f = (f_s/N)\{0, 1, 2, \cdots, N\}$ and N is the sequence length. The lower curve and the upper curve correspond to the phase slope of the air–glass interface and that of the glass–air interface, respectively. The shift from the lower curve to the upper curve at the central wavelength is the optical thickness of the microscope slide. The signal outside the 22-nm spectral bandwidth of the light source is dominated by noise.

B. Group Dispersion

The group dispersion of water at 820 nm was calculated from Eq. (15):

$$\left.\frac{dn_g}{d\lambda}\right|_{H_2O} = -\frac{1}{T}\frac{2\pi}{\lambda_s^2}\left(\left.\frac{d^2\phi}{dk^2}\right|_{\text{cuv}} - \left.\frac{d^2\phi}{dk^2}\right|_{H_2O_{\text{in cuv}}}\right)$$
$$= -1.23(\text{S.D.}\ \pm 0.30) \times 10^{-5}\ \text{nm}^{-1},$$

where S.D. is the standard deviation, the geometrical thickness is $T = 1.0$ cm (S.D. ± 50 μm), $[(2\pi)/T\lambda_s^2)][d^2\phi(k)/dk^2]|_{H_2O_{\text{in cuv}}} = 0.57(\text{S.D.} \pm 1.22) \times 10^{-5}\ \text{nm}^{-1}$, and $[(2\pi/T\lambda_s^2)][d^2\phi(k)/dk^2]|_{\text{cuv}} = 1.85(\text{S.D.} \pm 0.76) \times 10^{-5}\ \text{nm}^{-1}$. The group-dispersion error was calculated at a 95% confidence interval. Assuming that the variances of the two populations are equal, the 95% confidence interval was found such that $t_{1-\alpha/2}S_p(1/N_1 + 1/N_2)^{1/2}$, where S_p^2 is the estimated common pooled variance: $S_p^2 = [(N_1 - 1)\text{S.D.}_1^2 + (N_2 - 1)\text{S.D.}_2^2]/[N_1 + N_2 - 2]$, where the subscript 1 and the subscript 2 denote the empty cuvette and the cuvette filled with water, respectively, S.D. is the standard deviation of $(1/T)(2\pi/\lambda_s^2)(d^2\phi/dk^2)$, and N is the number of A-scans ($N_1 = N_2 = 100$).

Figure 4 illustrates typical interference signals from the coated mirror with and without the 1-cm-thick layer of water. Water dispersion increased the coherence length by 4 μm. The previously published value for the group dispersion of water in the range 810–860 nm was $-1.62(\pm 0.06) \times 10^{-5}\ \text{nm}^{-1}$.[13] Our laboratory room temperature, which was 25°, might have caused the discrepancy between the two measured group dispersions because the refractive index of water is a function of temperature as well.

The group dispersion of ZnSe at 820 nm was calculated:

$$\left.\frac{dn_g}{d\lambda}\right|_{\text{ZnSe}} = -\frac{1}{T}\frac{2\pi}{\lambda_s^2}\left(\left.\frac{d^2\phi}{dk^2}\right|_{\text{none}} - \left.\frac{d^2\phi}{dk^2}\right|_{\text{ZnSe disk}}\right)$$
$$= -38.58(\pm 1.23) \times 10^{-5}\ \text{nm}^{-1},$$

where the geometrical thickness, $T = 2.080(\text{S.D.} \pm 0.005) \times 10^6$ nm, was measured with a micrometer, $[(2\pi)/(T\lambda_s^2)][d^2\phi(k)/dk^2]|_{\text{none}} = 11.53(\text{S.D.} \pm 4.19) \times 10^{-5}\ \text{nm}^{-1}$, and $[(2\pi)/(T\lambda_s^2)][d^2\phi(k)/dk^2]|_{\text{ZnSe disk}} = -27.01(\text{S.D.} \pm 4.19) \times 10^{-5}\ \text{nm}^{-1}$. The error was calculated at a 95% confidence interval. Because ZnSe is more dispersive than water, the coherence length of the interference signal increased to 41 μm, as shown in Fig. 4. The group dispersion at 820 nm

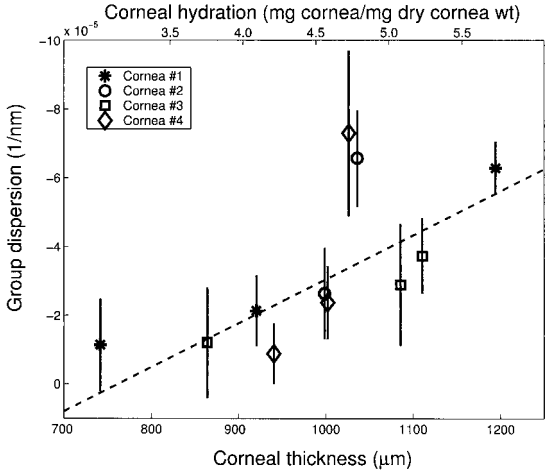

Fig. 5. Group dispersion of the cornea versus hydration and thickness. The error bars are 95% confidence intervals. Dashed curve, weighted least-squares regression. The intercept is 9.6(S.E. ± 4.0) × 10^{-5} nm^{-1}, and the slope is −13(S.E. ± 4) × 10^{-11} m^{-2}. The hydration is defined by the ratio of the water weight to the completely dry weight of the cornea.

of ZnSe, which was estimated numerically from a Sellmeier dispersion curve,[29] is -41.1×10^{-5} nm^{-1}.

The group dispersions of the four corneas under various hydrations are shown in Fig. 5. Group dispersion increased with hydration. A linear relationship between corneal thickness and group dispersion was calculated by weighted least-squares regression. The weighted least-squares involved finding $\tilde{a}$ and $\tilde{b}$ to minimize $\sum_i w_i[(dn_g/d\lambda)_i - (\tilde{a} + \tilde{b}T_i)]^2$,[30] where the inverse of the error was used for w_i at each thickness. The intercept, $\tilde{a}$, was 9.57(S.E. ± 3.96) × 10^{-5} nm^{-1}, and the slope, $\tilde{b}$, was −0.0128(S.E. ± 0.0039) × 10^{-8} m^{-2}. The t value for the null hypothesis that the slope, $\tilde{b}$, was equal to zero is 2.42 and the corresponding P value is 0.010. Thus the group dispersion of the cornea is significantly dependent on the corneal hydration.

5. Discussion

A. Comparison of Time Domain and Frequency Domain

Figures 2 and 3 show that the optical thickness is equal to the shift of the phase slope. Therefore the optical thickness can be calculated either in the time domain or in the frequency domain. In the time domain, usually the interference signal is demodulated to produce the envelope by use of either hardware (i.e., a lock-in amplifier) or software (i.e., quadrature-amplitude demodulation). In the frequency domain, finding the phase of the interference signal typically requires a phase-unwrapping algorithm because of the 2π ambiguity. However, we demonstrated that the first-order derivative of a phase with wave number can be calculated by use of Eq. (8) without a phase-unwrapping algorithm. There are two advantages to using the frequency domain for finding the optical thickness. First, no demodulation is required. Second, the sampling rate of a data acquisition board can be reduced to the Nyquist rate without compromising the accuracy of the measurement.[23]

B. Group Dispersion as an Indicator of Physiological Condition

The cornea is composed of stroma lamellae, which are long, parallel, and cylindrical collagen fibrils, immersed in a ground substance. The collagen fibrils are uniform in diameter, and the spacing between the adjacent fibrils in the bundle is approximately 50–60 nm.[31] It is known that the changes in hydration in the cornea take place only in the ground substance between the fibrils[31]; that is, the volume of the collagen fibrils in the cornea is constant when hydration increases. There could be two basic reasons that a change in corneal hydration causes a change in dispersion. First, as the cornea is hydrated the volume fraction of water in the cornea increases. A difference in dispersion of the water and the nonwater components of the cornea thereby leads to a change in measured dispersion when the cornea is hydrated. Second, a change in interfibrilar spacing may result in an increase in group dispersion, in which case the group dispersion may be an indicator of the spatial organization of the collagen fibrils. Given that the corneal thickness is linearly proportional to corneal hydration,[27] and that hydration affects dispersion, one expects a monotonic relationship between hydration and dispersion. Our study of the relationship between the group dispersion of the cornea and the corneal hydration shows that the group dispersion is significantly dependent on the water content. Thus the group dispersion can be a tool with which to measure and monitor corneal hydration and the spatial organization of collagen fibrils. Information about corneal hydration is essential for that diagnosis of ocular diseases and for surgical planning and monitoring. For example, the corneal hydration affects

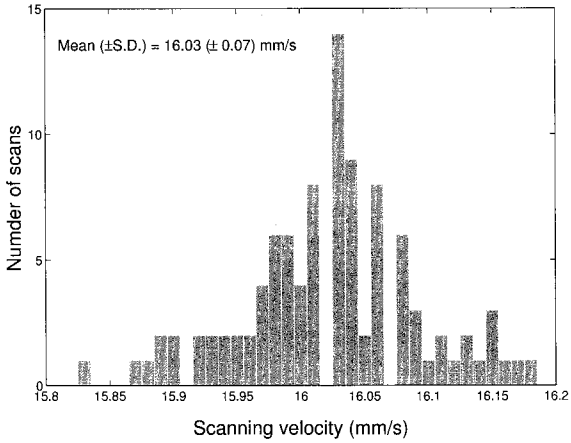

Fig. 6. Actual scanning speed distribution of 100 A scans. Each scanning speed was calculated from the peak of the spectral power density of each interference signal. Although the scanning speed was set at 16 mm/s, the actual speed varied as shown.

the eximer laser ablation rate in excimer laser keratorefractive surgery.[32]

C. Importance of Constant Scanning Velocity

A constant scanning velocity is required for an accurate dispersion calculation because the distance interval of each sampled point is defined by V/f_s, where V is the scanning speed and f_s is the sampling frequency. High-speed scanning of the mirror in the reference arm is necessary in biological samples that must be scanned rapidly to reduce artifacts caused by cardiac motion, respiration, and dehydration. Figure 6 shows that the actual scanning speed of each A scan fluctuated, although the scanning velocity and the sampling rate were set at a constant speed as 16 mm/s and 1 MHz, respectively. This variation in scanning velocity appears to be a significant error for our dispersion calculation.

6. Conclusions

In standard OLCR or OCT, accurate phase quantification of the interference signal is hampered by phase noise. However, we have demonstrated that the first (i.e., the phase slope) and the second derivatives of the interference signal with respect to wave number can be calculated by discrete-time signal processing in the frequency domain. The shift of the phase slope of a transparent sample was shown to be equal to the optical thickness. The group dispersion can be obtained by use of the phase slope and the second derivative. We demonstrated that the group dispersion of the cornea was significantly dependent on hydration, indicating that group dispersion can be a potential tool with which to measure the corneal hydration.

This research was supported by grants NIH EY 13015 and NIH EYE 09714 from the National Institutes of Health.

References

1. D. Huang, E. A. Swanson, C. P. Lin, J. S. Schuman, W. G. Stinson, W. Chang, M. R. Hee, T. Flotte, K. Gregory, C. A. Puliafito, and J. G. Fujimoto, "Optical coherence tomography," Science **254,** 1178–1181 (1991).
2. A. F. Fercher, "Optical coherence tomography," J. Biomed. Opt. **1,** 157–173 (1996).
3. J. M. Schmitt, "Optical coherence tomography (OCT): a review," IEEE J. Sel. Top. Quantum Electron. **5,** 1205–1215 (1999).
4. X. J. Wang, T. E. Milner, Z. Chen, and J. S. Nelson, "Measurement of fluid-flow-velocity profile in turbid media by the use of optical Doppler tomography," Appl. Opt. **36,** 144–149 (1997).
5. J. A. Izatt, M. D. Kulkarni, S. Yazdanfar, J. K. Barton, and A. J. Welch, "*In vivo* bidirectional color Doppler flow imaging of picoliter blood volumes using optical coherence tomography," Opt. Lett. **22,** 1439–1441 (1997).
6. M. R. Hee, D. Huang, E. A. Swanson, and J. G. Fujimoto, "Polarization-sensitive low-coherence reflectometer for birefringence characterization and ranging," J. Opt. Soc. Am. B **9,** 903–908 (1992).
7. J. F. de Boer and T. E. Milner, "Review of polarization sensitive optical coherence tomography and Stokes vector determination," J. Biomed. Opt. **7,** 359–371 (2002).
8. S. Jiao and L. H. Wang, "Two-dimensional depth-resolved Mueller matrix of biological tissue measured with double-beam polarization-sensitive optical coherence tomography," Opt. Lett. **27,** 101–103 (2002).
9. U. Morgner, W. Drexler, X. Kärtner, X. D. Li, C. Pitris, E. P. Ippen, and J. G. Fujimoto, "Spectroscopic optical coherence tomography," Opt. Lett. **25,** 111–113 (2000).
10. P. A. Edney and J. T. Walsh, "Acoustic modulation and photon–photon scattering in optical coherence tomography," Appl. Opt. **40,** 6381–6388 (2001).
11. W. V. Sorin and D. F. Gray, "Simultaneous thickness and group index measurement using optical low-coherence reflectometry," IEEE Photon. Technol. Lett. **4,** 105–107 (1992).
12. G. J. Tearney, M. E. Brezinski, J. F. Southern, B. E. Bouma, M. E. Hee, and J. G. Fujimoto, "Determination of the refractive index of high scattering human tissue by optical coherence tomography," Opt. Lett. **20,** 2258–2260 (1995).
13. W. Drexler, C. K. Hitzenberger, A. Baumgartner, O. Findl, H. Sattmann, and A. Fercher, "Investigation of dispersion effects in ocular media by multiple wavelength partial coherence interferometry," Exp. Eye Res. **66,** 25–33 (1998).
14. B. E. Bouma, G. J. Tearney, S. A. Boppart, M. R. Hee, M. E. Brezinski, and J. G. Fujimoto, "High-resolution optical coherence tomographic imaging using a mode-locked Ti:Al_2O_3 laser source," Opt. Lett. **20,** 1486–1488 (1995).
15. C. K. Hitzenberger, A. Baumgartner, and A. F. Fercher, "Dispersion induced multiple signal peak splitting in partial coherence interferometry," Opt. Commun. **154,** 179–185 (1998).
16. C. K. Hitzenberger, A. Baumgartner, W. Drexler, and A. F. Fercher, "Dispersion effects in partial coherence interferometry: implications for intraocular ranging," J. Biomed. Opt. **4,** 144–151 (1999).
17. M. D. Kulkarni, C. W. Thomas, and J. A. Izatt, "Image enhancement in optical coherence tomography using deconvolution," Electron. Lett. **33,** 1365–1367 (1997).
18. D. L. Marks, A. L. Oldenburg, J. J. Reynolds, and S. A. Boppart, "Digital algorithm for dispersion correction in optical coherence tomography for homogeneous and stratified media," Appl. Opt. **42,** 204–217 (2003).
19. J. F. de Boer, C. E. Saxer, and J. S. Nelson, "Stable carrier generation and phase-resolved digital data processing in optical coherence tomography," Appl. Opt. **40,** 5787–5790 (2001).
20. W. H. Steel, *Interferometry* (Cambridge U. Press, Cambridge, 1983), pp. 256–257.
21. D. P. Dave and T. E. Milner, "Optical low-coherence reflectometer for differential phase measurement," Opt. Lett. **25,** 227–229 (2000).
22. M. A. Schofield and Y. Zhu, "Fast phase unwrapping algorithm for interferometric applications," Opt. Lett. **28,** 1194–1196 (2003).
23. B. L. Danielson and C. Y. Boisrobert, "Absolute optical ranging using low coherence interferometry," Appl. Opt. **30,** 2975–2979 (1991).
24. A. V. Oppenheim, R. W. Schafer, and J. R. Buck, *Discrete-Time Signal Processing* (Prentice-Hall, Upper Saddle River, N.J., 1999).
25. R. N. Bracewell, *The Fourier Transform and Its Applications* (McGraw-Hill, New York, 1978), pp. 189–194.
26. A. Wexler, "Constant humidity solutions," in *Handbook of Chemistry and Physics*, D. R. Lide, ed. (CRC, Boca Raton, Fla., 2000), Sec. 15–25.
27. B. Hedbys and S. Mishima, "The thickness–hydration relationship of the cornea," Exp. Eye Res. **5,** 221–228 (1966).
28. I. Fatt and T. K. Goldstick, "Dynamics of water transport in swelling membranes," J. Colloid. Sci. **20,** 962–989 (1965).

29. W. I. Tropf, M. E. Thomas, and T. J. Harris, "Properties of crystals and glasses," in *Handbook of Optics*, M. Bass, ed. (McGraw-Hill, New York, 1995), Vol. 2, Chap. 33.
30. N. R. Draper and H. Smith, *Applied Regression Analysis* (Wiley, New York, 1981).
31. D. M. Maurice, "The cornea and sclera," in *The Eye*, H. Davson, ed. (Academic, Orlando, Fla., 1984), pp. 1–158.
32. P. J. Dougherty, K. L. Wellish, and R. K. Maloney, "Excimer laser ablation rate and corneal hydration," Am. J. Ophthalmol. **118,** 169–176 (1994).